Supporting Online Material for

Structural basis of TLR5-flagellin recognition and signaling

Sung-il Yoon[1], Oleg Kurnasov[2†], Venkatesh Natarajan[3†], Minsun Hong[1†], Andrei V. Gudkov[3,4], Andrei L. Osterman[2 *], Ian A. Wilson[1,5 *]

[1]Department of Molecular Biology and [5]the Skaggs Institute for Chemical Biology, The Scripps Research Institute, La Jolla, CA 92037, USA

[2]Sanford-Burnham Medical Research Institute, La Jolla, CA 92037, USA

[3]Roswell Park Cancer Institute, Buffalo, NY 14263, USA

[4]Cleveland BioLabs, Inc. (CBLI), Buffalo, NY14203, USA.

[†] These authors contributed equally to this work

[*] To whom correspondence should be addressed. E-mail: wilson@scripps.edu (I.A.W.), osterman@sanfordburnham.org (A.L.O.)

This PDF file includes

Materials and Methods

Protein expression and purification

To obtain recombinant proteins of TLR5 ectodomain in a quantity suitable for biophysical and structural studies, we screened human, mouse, frog, trout, and zebrafish TLR5 orthologs for recombinant expression using a baculovirus expression system. Only zebrafish TLR5b ectodomain (TLR5-ECD; residues 22-652) could be expressed, but its yield after purification was not sufficient for structural studies. To improve protein yield and crystallizability, a hybrid method (*20*) was applied in which the N- or C-terminal region of zebrafish TLR5b was replaced with that of hagfish VLR B.61. Three chimeras, including TLR5-N6$_{VLR}$ (TLR5 residues 22-181; VLR residues 134-200), TLR5-N12$_{VLR}$ (TLR5 residues 22-342; VLR residues 126-200), and TLR5-N14$_{VLR}$ (TLR5 residues 22-390; VLR residues 126-200) (fig. S2A), were sufficiently expressed in monomeric forms and, thus, used for crystallographic and FliC binding studies.

To prepare TLR5-ECD and TLR5$_{-VLR}$ chimeric constructs, TLR5- and VLR-encoding DNAs were amplified by PCR and ligated into a modified pAcGP67 transfer vector that contains C-terminal thrombin cleavage site, Strep-Tactin II tag, and His$_6$ tag. The transfer vector DNA was co-transfected with a linearized baculovirus DNA, Profold-ER1 (AB vector), into Sf9 insect cells. TLR5-expression baculovirus was amplified in Sf9 cells and TLR5 expression was carried out for two days after baculovirus infection in Hi5 insect cells. TLR5 was purified in three steps using Ni-NTA affinity, Strep-Tactin affinity, and size-exclusion chromatography. Thrombin digestion was performed before size-exclusion chromatography purification step to remove the C-terminal expression and purification tags.

The zebrafish TLR5 used for this study was derived from an EST clone (GenBank accession number EB937163; Open Biosystems) that contains 12 amino-acid sequence changes (V24E, L124V, Q159K, R227K, S229T, D334N, N392K, E503G, G583S, S615P, R634K, and D641N), compared to the published reference sequence (GeneBank accession number NM001130595). Six sequence changes (V24E, L124V, Q159K, R227K, S229T, and D334N) in TLR5-N14 (residues 22-390) are not in the TLR5-N14$_{VLR}$/FliC binding interface. Thus, we believe that the observed polymorphism does not compromise our interpretation on the TLR5-FliC interaction. Since this TLR5 EST clone yielded higher protein expression, it was used throughout.

The full-length FliC (residues 1-504) from *Salmonella enterica* subspecies *enterica* serovar Dublin and its variants including FliC-ΔD0 (residues 47-465), CBLB502 (residues 1-175, a 16-residue linker, residues 401-504) and CBLB502-ΔD0 (residues 53-175, a 16-residue linker, residues 401-460) (fig. S2B) were expressed in *Escherichia coli* cells using an expression vector, pET49b, as previously described (*36*). FliC was attached to an N-terminal His$_6$-tag and thrombin or enterokinase cleavage site. FliC recombinant protein expression was induced at log phase for 3 hours in the presence of 1 mM IPTG in T7 Express I^q *E. coli* cells (New England Biolabs). Cells were lysed with a high-pressure EmulsiFlex-C3 homogenizer (Avestin) or sonication and the resulting material was centrifuged. FliC, FliC-ΔD0, and CBLB502-ΔD0 proteins were purified from the supernatant by Ni-NTA affinity and size-exclusion chromatography. CBLB502 protein was collected from inclusion bodies, solubilized in 2 M urea, and purified by Ni-NTA affinity and size-exclusion chromatography.

To prepare TLR5-N14$_{VLR}$/FliC-ΔD0 complex proteins, TLR5-N14$_{VLR}$ obtained from Strep-Tactin column was mixed with the purified FliC-ΔD0 in a 1:1 molar ratio. After removal

of the C-terminal tags of TLR5-N14$_{VLR}$ and the N-terminal tag of FliC-ΔD0 by thrombin, the resulting complex was further purified by size-exclusion chromatography.

Crystallization and data collection

Crystals of TLR5-N6$_{VLR}$, TLR5-N12$_{VLR}$, and TLR5-N14$_{VLR}$/FliC-ΔD0 were generated by the sitting drop, vapor diffusion method. TLR5-N6$_{VLR}$ crystals were obtained at 23ºC by mixing 0.5 µl of protein and 0.5 µl of 10% PEG6000/0.1 M Tris pH 8.5, and cryo-protected in 25% ethylene glycol. Diffraction data were collected at 100K at the Advanced Photon Source (APS) beamline 23ID-D. TLR5-N12$_{VLR}$ crystals were formed at 4ºC in a drop of 0.1 µl of protein and 0.1 µl of 20% MPD/0.1 M Hepes pH 7.0, and were cryo-cooled in the presence of 28% MPD. Diffraction data were collected at the Stanford Synchrotron Radiation Lightsource (SSRL) beamline 11-1. TLR5-N14$_{VLR}$/FliC-ΔD0 was crystallized at 23ºC in a drop containing 0.5 µl of protein and 0.5 µl of 15% PEG8000/0.2 M magnesium chloride/0.1 M Tris pH 8.5, and crystals were cryo-protected in a 50:50 paratone-N:paraffin mix. Diffraction data were collected at the APS beamline 23ID-B. All diffraction data were processed with *HKL2000* (*42*).

Structure determination and refinement

The TLR5-N6$_{VLR}$ structure was determined by molecular replacement with *PHASER* (*43*) using the C-terminal region of hagfish VLR B.61 (*44*) as a search model. The TLR5-N12$_{VLR}$ structure was determined by molecular replacement using the TLR5 segment of the partially refined TLR5-N6$_{VLR}$ structure. The TLR5-N14$_{VLR}$/FliC-ΔD0 was determined by molecular replacement using the TLR5-N12 structure and *st*FliC D1 domain structure (*40*) as search models. The structure models were iteratively built with *COOT* (*45*) and refined with *REFMAC5* (*46*). FliC-ΔD0 used for TLR5-N14$_{VLR}$/FliC-ΔD0 structure determination contains D1, D2, and D3 domains, but the D3 domain could not be built in the complex structure due to extremely poor electron density, which likely reflects disorder in this domain.

Competitive fluorescence polarization (FP) assays

To address primary binding of TLR5-ECD (or its variants) to CBLB502 (or its mutants), fluorescence polarization assays were applied using DTX880 multimode plate reader (Beckman Coulter). Purified CBLB502 protein was labeled by N-hydroxysuccinimide (NHS)-fluorescein (Thermo Scientific) in PBS buffer at room temperature for 2 hours. Unbound dye was removed using a size-exclusion column. Efficiency of fluorescein conjugation to CBLB502 was experimentally determined as ~0.9 of fluorescein-to-protein ratio using the molar extinction coefficient of NHS-fluorescein, 70,000 $M^{-1}cm^{-1}$. The direct binding of fluorescein-labeled CBLB502 to TLR5-ECD or TLR5-N14$_{VLR}$ was detected, but accurate K_d values could not be derived from this assay due to sensitivity limitation at sub-nanomolar concentration. Instead, IC_{50} values were determined in a competition binding assay where serially diluted CBLB502 or its mutants were added into a mixture of 25 nM TLR5-ECD (or TLR5-N14$_{VLR}$) and 25 nM fluorescein-labeled CBLB502.

NF-κB-dependent luciferase reporter and NF-κB-dependent GFP reporter assays

Reporter cells, that constitutively express human TLR5 and produce NF-κB-dependent luciferase (or GFP) in response to extrinsically added FliC, were generated by lentiviral transduction of HEK293 cells. For luciferase assays, 50,000 reporter cells were seeded in each well of a 96-well white clear-bottom plate (Costar) and incubated overnight. Purified CBLB502

or mutant proteins were serially diluted, and added into wells. After 8-hour stimulation, luciferase activity was immediately measured with Bright-Glo reagent (Promega) using a plate reader (Wallac). In GFP assays, the percentage of GFP-positive cells was determined by flow cytometric analysis. For competitive reporter assays, a mixture of CBLB502 (60-120 pM) and serially diluted TLR5-ECD (or its variants) was added to reporter cells.

SOM Text

Significance of the current study

Activation of the NF-κB pathway, which leads to the generation and release of various types of prosurvival and proinflammatory factors, is one of the key common signaling mechanisms for TLRs. Remarkably, the exact repertoire of induced factors and the physiological consequences of TLR-triggered responses differ for each agonist-receptor pair, which is reflected, at least partially, in differential expression of TLRs in various tissues and cell types. Thus, lipopolysaccharide (LPS), a TLR4 agonist, is known to be a major factor causing septic shock, whereas FliC has a relatively mild inflammatory effect while inducing a number of beneficial immunostimulatory, antiinfective and antiapoptotic effects (*47*). TLR5 interaction with FliC or its pharmacologically optimized derivative, CBLB502 (fig. S2B), protects the hematopoietic system and gastrointestinal tissues from radiation-induced damage, creating opportunities for therapeutic applications (*36*). On the other hand, TLR5 hyperactivation has been implicated in Crohn's disease (*48*). Therefore, structural and mechanistic understanding of TLR5-FliC interaction would impact currently developing as well as new biomedical applications, such as antagonistic therapeutics against certain hyper-inflammatory syndromes (*49*).

Previous mutational studies suggested that the conserved D1 domain of FliC (D0-D1-D2-D3) plays a key role in functional interactions with TLR5 (*11, 50-52*). In contrast, the D2-D3 hypervariable domains of FliC are dispensable for TLR5 binding or signaling, as CBLB502 (consisting only of D0-D1) displays the same NF-κB activation and radioprotection efficiency as its parent FliC (*36*). However, how these FliC domains interact with TLR5 remains to be elucidated (*38, 53-54*). This lack of structural information and of direct *in vitro* binding data (beyond cell-based signaling assays) have precluded mechanistic analysis of TLR5-FliC recognition and signaling.

Here, we report the crystal structure of a complex between the N-terminal 14 LRR modules of zebrafish TLR5 and D1-D2 domains of FliC, and validate our model on the TLR5 recognition and mechanism by structure-guided mutational studies on CBLB502. Our structural, biophysical, and cellular studies on the TLR5-flagellin interaction highlights a novel mechanism for protein-ligand recognition by a TLR and provides deeper insights into TLR-mediated activation of innate immunity. Furthermore, new insights obtained from this study would provide valuable templates for improvement of current drugs under clinical trials (a radioprotection drug, CBLB502, or a flu vaccine, VAX102), and for development of novel therapeutic applications such as vaccine adjuvants or antagonistic therapeutics for hyper-inflammatory diseases.

Unique mode of ligand recognition by TLR5, but with some structural similarity to TLR4 binding to MD-2^{LPS}

Despite evolutionary and structural relatedness between TLR5 and TLR3 (fig. S4), their cognate ligand binding mechanisms are completely different in many aspects (fig. S1). In the TLR3/dsRNA complex, one dsRNA molecule is sandwiched between two TLR3 chains, forming a bridge in the 1:2 complex (*3*). TLR3 uses its distantly located, N-terminal and C-terminal

ascending lateral surfaces from LRRNT-LRR3 and LRR19-LRR23, respectively, in RNA recognition without engaging the central region (fig. S1A). In comparison, TLR5 forms an activated 2:2 complex with FliC where each FliC buttresses the TLR5 homodimer on its outside rather than traversing between the two TLR molecules (Fig. 2A and fig. S1D). TLR5 recognizes FliC using the ascending lateral surface of TLR5 at LRRNT-LRR10 and their proximal convex surface of TLR5′ at LRR12-LRR13.

Further structure comparison with LPS-bound TLR4 (*5*) and lipopeptide-bound TLR1/2 (*4*) underscores the uniqueness of TLR5 in its ligand recognition. Unlike TLR5, TLR4 requires a co-receptor, MD-2, that provides the LPS binding site, for LPS antigen recognition (fig. S1C). TLR5 mainly uses hydrophilic surfaces exposed on its lateral and convex sides for ligand binding, whereas TLR1/2 employ long hydrophobic pockets housed between their central and C-terminal LRR subdomains to enclose acyl chains of a lipopeptide ligand (fig. S1B). Taken together, unlike other non-protein ligand binding TLRs, TLR5 employs a unique structural mechanism for protein ligand recognition.

Although TLR5 and TLR4 completely differ in antigen recognition mechanisms, their protein-protein interaction modes [TLR5 binding to FliC ligand protein versus TLR4 binding to MD-2 co-receptor protein complexed with LPS (MD-2^{LPS})] share three structural features (fig. S14). First, they both form complexes with a 2:2 molecular stoichiometry (fig. S14A). Second, FliC and MD-2^{LPS} reside on and protrude from the ascending lateral side of one TLR via the primary binding interface, and are located on the concave surface of the other TLR via the secondary dimerization interface. Last, the LRR9 loops of TLR5 and TLR4 are both employed for the primary interaction and the relative positioning of their interfaces is similar (fig. S14B). Nevertheless, a significant difference is found in the interface residues due to the different nature of their binding protein partners, such as shape and size (fig. S14B). MD-2 is a small globular protein and is snuggly enclosed mainly by the concave surface of TLR4, whereas FliC D1 domain in an elongated structure is recognized primarily by the lateral surface of TLR5.

Contribution of the FliC D0 domain and the TLR5-ECD C-terminal region to the TLR5-FliC interaction

We note that the TLR5-N14/FliC-ΔD0 structure inevitably provides a partial view on dimerization. Our data clearly suggest that the FliC domain D0 plays an important role in signaling, most likely via its contribution to the 2:2 complex as its contribution to the 1:1 complex is minimal. To assess a possible contribution of the D0 domain to TLR5 dimerization, we superimposed the full-length cryo-EM model of FliC that was derived from flagellar filaments (*55*), onto our structure. Based on this model, the D0 domain would point downward clashing with a tentative location of the cell membrane. Thus, D0 would adopt different configuration when bound to TLR5, compared to that observed in flagellar filament. The long, rod-shaped D0 is expected to change its orientation through a flexible interdomain D0-D1 hinge upon TLR5 binding, which would potentially allow it to reach the opposing 1:1 complex and facilitate TLR5 dimerization. However, we cannot rule out other possible mechanisms such as engagement of D0 in recruitment of currently unknown adaptor or co-receptor molecules for TLR5 activation on the cell surface.

Our structure comparison and modeling suggest that TLR5's C-terminal LRRs, which were replaced by the capping region of VLR to improve TLR5 expression, are likely to contribute to the formation of the 2:2 complex. An additional secondary dimerization interface-α that extends from interface-α of the complex structure would be formed between TLR5 LRR15-

LRR16 and a FliC loop (residues 130-135), which is located at the C-terminal end of αND1b. This is supported by an additional decrease in signaling of DIM2 (deletion of residues 126-128 to disrupt the 130-135 loop structure), compared to DIM1 and DIM1b (Fig. 1C and table S3). Moreover, secondary dimerization interface-β at LRR12/13 can be extended to the C-terminal LRRs in a similar manner to the structurally related TLR complex, TLR4/MD-2^{LPS}, where LRR13 to LRR21 contribute extensively to the TLR4-TLR4′ interface (*5*).

Primary binding interface observed in the TLR5-$N14_{VLR}$/FliC-ΔD0 complex structure

The TLR5-$N14_{VLR}$/FliC-ΔD0 complex structure can provide a model to understand the mechanism of FliC-induced TLR5 activation. Although partial fragments of TLR5 and FliC were used for structure determination, our structure undoubtedly presents the complete primary binding interface for the following reasons. First, the hypervariable D2 and D3 domains are not involved in TLR5 interactions in the complex structure in agreement with previously published data (*11, 50-52*). The D3 domain is, in fact, disordered in the complex structure, and does not interact with TLR5, given that its electron density envelope is located above D2 and quite distant from TLR5. Second, TLR5-ECD exhibits very similar primary binding affinities for CBLB502 and CBLB502-ΔD0 as TLR5-$N14_{VLR}$, suggesting essentially no energetic contribution of the D0 domain to primary binding (fig. S12). Last, deletion of the C-terminal region (LRR14-LRRCT) in TLR5-ECD does not substantially reduce CBLB502 binding in competitive NF-κB reporter assays (Fig. 1B and fig. S10, E and F). These results demonstrate that primary binding occurs exclusively through TLR5 LRRNT-LRR10 and FliC D1 as described in the complex structure.

Fig. S1

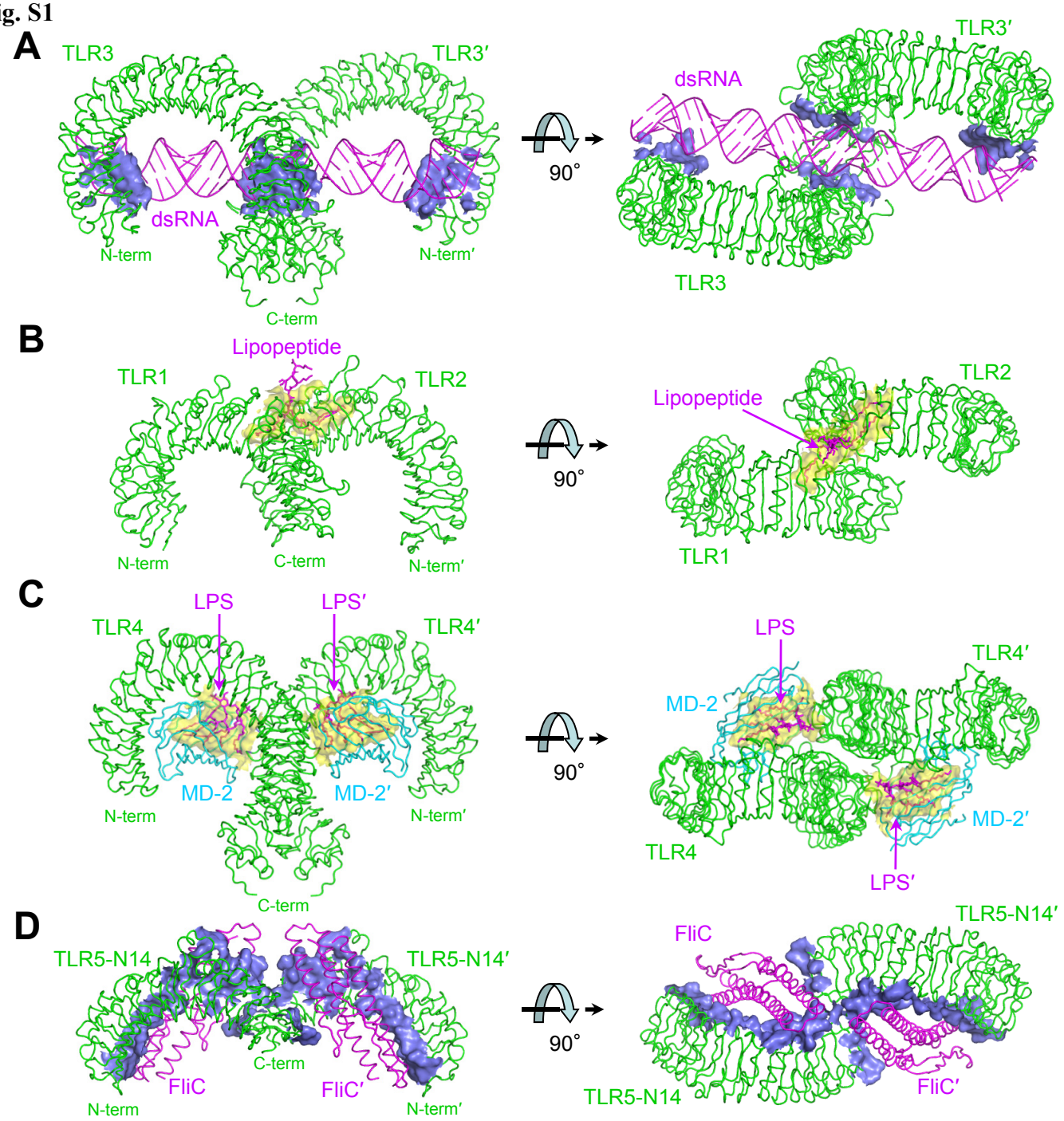

Fig. S1. Different ligand recognition by TLRs but common tail-to-tail dimer organization. TLR3 interacts with viral double-stranded RNA through its hydrophilic lateral surface (light blue surface) (A; PDB code 3CIY) (*3*) whereas TLR1/2 bind their ligands between TLR1 and TLR2 on the convex face and partially enclose their lipopeptide ligand tails using internal hydrophobic pockets (yellow surface) on each TLR (B; PDB code 2Z7X) (*4*). TLR4 recognizes lipopolysaccharide via presentation by a hydrophobic cavity (yellow surface) of a co-receptor MD-2 (C; PDB code 2Z7X) (*5*). For comparison, the crystal structure of FliC-ΔD0-bound TLR5-N14 homodimer that has been determined for this study is also shown (D). TLR5 mainly recognizes its ligand, FliC, using the exposed hydrophilic surface (light blue) of the D1 domain. Despite such diverse ligand-specific recognition mechanisms, all the agonist-activated TLR structures form a similar dimer organization in a tail-to-tail orientation, which brings the C-terminal regions of two TLR ectodomains into juxtaposition so that their intracellular TIR domains can initiate the cell signaling cascades.

Fig. S2

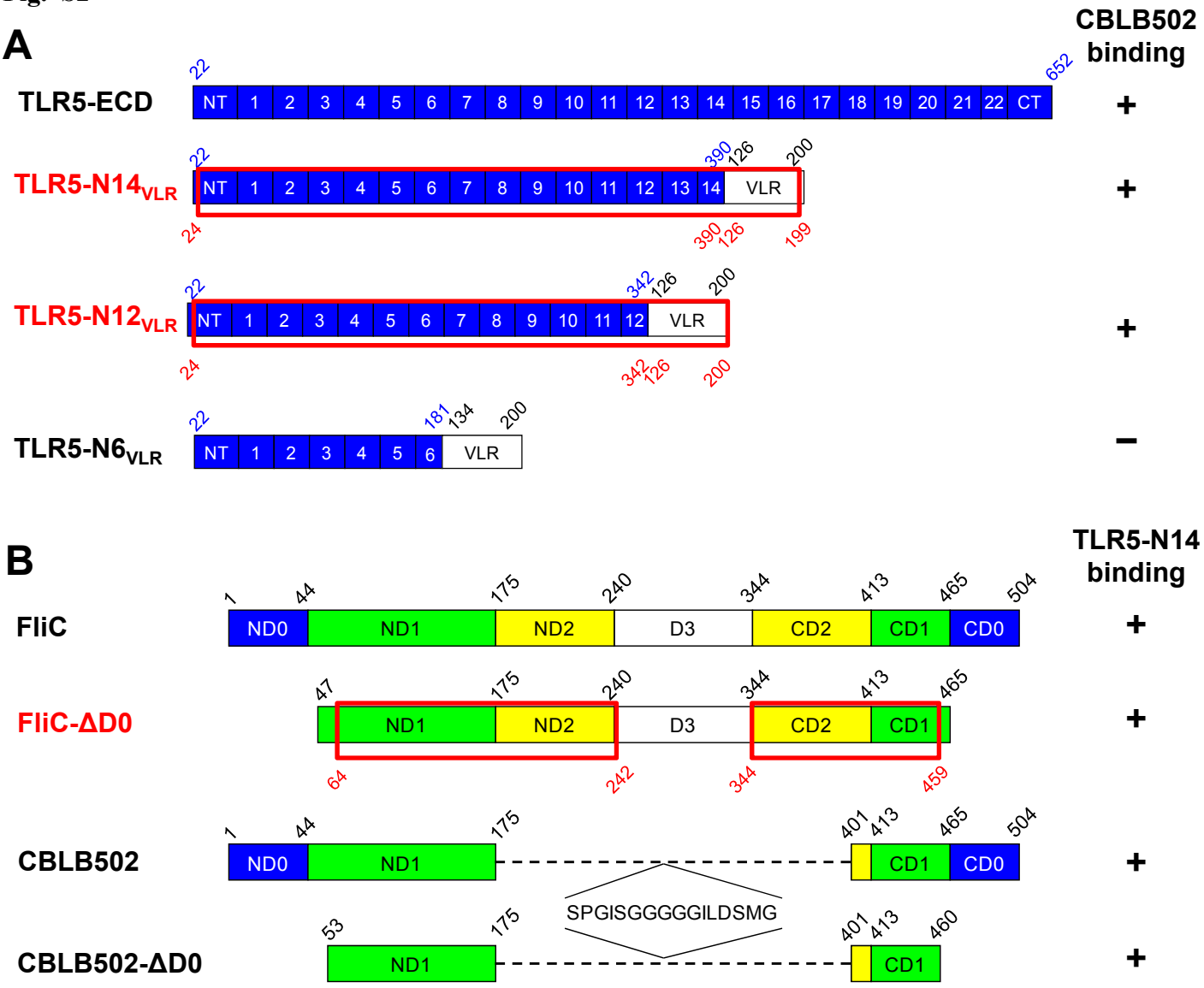

Fig. S2. TLR5-FliC constructs and interactions.
(A) TLR5-ECD and TLR5-VLR chimeras. The N-terminal LRR modules of *dr*TLR5 and the C-terminal VLR B.61 capping region are shown by blue and white boxes, respectively. Residue numbers at N/C-terminal ends of TLR5 and VLR used for the constructs are shown above the LRR module boxes. Models built in the crystal structures of TLR5-$N14_{VLR}$/FliC-ΔD0 and TLR5-$N12_{VLR}$ are highlighted by red boxes along with terminal residue numbers shown below the boxes. The initial qualitative assessment of CBLB502 binding (see Fig. 1A) is marked by "+" or "-". (B) *sd*FliC and its variants. FliC consists of two conserved D0 and D1 domains and two hypervariable D2 and D3 domains. Each of D1, D2, and D3 domains is constituted from two separate segments of the N-terminal region (ND) and the C-terminal region (CD). Domain boundary residues are shown above the domain boxes. The model built in the TLR5-$N14_{VLR}$/FliC-ΔD0 structure is delineated by red boxes along with terminal residue numbers. Interaction with TLR5-$N14_{VLR}$ was assessed as reflected by "+" or "-". In CBLB502, the hypervariable region (D2-D3) is replaced by a 16-residue linker.

Fig. S3

```
LRRNT
Human       IPSCSFDGRIAFYRFCNLTQVPQVLN-    46
Bovine      MSSCFFDGWRAIYLSCNLTQVPQVPN-    46
Mouse       ISPCSSDGRIAFFRGCNLTQIPWILNT    47
Chicken     SRSCYSEDQVSMYNSCNLTGVPPVPK-    47
Zebrafish   TSECSVIGYNAICINRGLHQVPELPA-    47

LRR1        xLxxLxLxxNxϕxxϕxxxxFxxLx
Human       TTERLLLSFNYIRTVTASSFPFLE       70
Bovine      TTKSLLLSFNYIRTVTTASFPFLE       70
Mouse       TTERLLLSFNYISMVVATSFPLLE       71
Chicken     DTAKLFLTYNYIRQVTATSFPLLE       71
Zebrafish   HVNYVDLSLNSIAELNETSFSRLQ       71

LRR2        xLxxLxLxxN-x--ϕxϕxxxxFxxLx
Human       QLQLLELGSQ-YTPLTIDKEAFRNLP     95
Bovine      QLQLLELGTQ-FTPLTIYREAFRNLP     95
Mouse       RLQLLELGTQ-YANLTIGPGAFRNLP     96
Chicken     DLFLLEIGTQRVFPLYIGKEAFRNLP     97
Zebrafish   DLQFLKVEQQ-TPGLVIRNNTFRGLS     96

LRR3        xLxxLxLxxNx-ϕxϕxxxxFxxLx
Human       NLRILDLGSSKIYFLHPDAFQGLF      119
Bovine      NLRILDLGGSQINFLHPDAFQGLP      119
Mouse       NLRILDLGQSQIEVLNRDAFQGLP      120
Chicken     NLRVLDLGFNNILLLDLDSFAGLQ      121
Zebrafish   SLIILKLDYNQFLQLETGAFNGLA      120

LRR4        xLxxLxLxxNxϕxx-ϕ-xxxxFxxLx
Human       HLFELRLYFCGLSDAVLKDGYFRNLK    145
Bovine      HLTKLRLFSCGLSDAVLKDGYFRNLA    145
Mouse       HLLELRLFSCGLSSAVLSDGYFRNLY    146
Chicken     RLTILRLFQNNLGDSILEERYFQDLR    147
Zebrafish   NLEVLTLTQCNLDGAVLSGNFFKPLT    146

LRR5        xLxxLxLxxNxϕxxϕxxxx-FxxLx
Human       ALTRLDLSKNQIRSLYLHPSFGKLN     170
Bovine      SLTHLDLSKNKIQSLYLHPSFRELN     170
Mouse       SLARLDLSGNQIHSLRLHSSFRELN     171
Chicken     SLEELDLSGNQITKLHPHPLFYNLT     172
Zebrafish   SLEMLVLRDNNIKKIQPASFFLNMR     171

LRR6        xLxxLxLxxNxϕxxϕxxxx---FxxL
Human       SLKSIDFSSNQIFLVCEHELEPLQGK    196
Bovine      SLKSIDFSFNKIPIVCEQEFKPLQGK    196
Mouse       SLSDVNFAFNQIFTICEDELEPLQGK    197
Chicken     ILKAVNLKFNKISNLCESNLTSFQGK    198
Zebrafish   RFHVLDLTFNKVKSICEEDLLNFQGK    197

LRR7        xLxxLxLxxNxϕxxx---------xxxxFxxL
Human       TLSFFSLAANSLYS-R-VSVDWGKCMNPFRNM    226
Bovine      TLSFLSLADNQLYS-R-VSVDWNKCLNPFRNM    226
Mouse       TLSFFGLKLTKLFS-R-VSVGWETCRNPFRGV    227
Chicken     HFSFFSLSTNTLYR-T-DKMIWAKCPNPFRNI    228
Zebrafish   HFTLLRLSSITLQDMNEYWLGWEKCGNPFKNT    229

LRR8        xLxxLxLxxNxϕxxxx---ϕxxxFxxL
Human       VLEILDVSGNGWTVDITGNFSNAISKS    253
Bovine      VLETLDVSGNGWGVDIMRNFSNAINGS    253
Mouse       RLETLDLSENGWTVDITRNFSNIIQGS    254
Chicken     TFNSLDVSENGWSTETVQYFCTAIKGT    255
Zebrafish   SITTLDLSGNGFKESMAKRFFDAIAGT    256

LRR9        xLxxLxLxxNx-ϕx--------x-ϕxxxxFxxL-x-
Human       QAFSLILAHHI-MGAGFGFHNIKDPDQNTFAGLARS    288
Bovine      QIFSLVLTRHI-MGSSFGFSNLKDPDYHTFAGLARS    288
Mouse       QISSLILKHHI-MGPGFGFQNIRDPDQSTFASLARS    289
Chicken     QINYLSFRSHT-MGSGFGFNNLKNPDTDTFTGLARS    290
Zebrafish   KIQSLILSNSYNMGSSFGHTNFKDPDNFTFKGLEAS    292

LRR10       xLxxLxLxxNxϕxxϕxxxxFxxLx
Human       SVRHLDLSHGFVFSLNSRVFETLK      312
Bovine      SMIQLDISHGYIFSVNFRIFETLQ      312
Mouse       SVLQLDLSHGFIFSLNPRLFGTLK      313
Chicken     DLHLLDISNGFIFSLNSLIFESLR      314
Zebrafish   GVKTCDLSKSKIFALLKSVFSHFT      316

LRR11       xLxxLxLxxNxϕxxϕxxxxFxxLx
Human       DLKVLNLAYNKINKIADEAFYGLD      336
Bovine      ELKVLNLAYNKINKIADEAFYGLD      336
Mouse       DLKMLNLAFNKINKIGENAFYGLD      337
Chicken     NLEFLNLFRNKINQIQKQAFFGLE      338
Zebrafish   DLEQLTLAQNEINKIDDNAFWGLT      340

LRR12       xLxxLxLxxNxϕxxϕxxxxFxxLx
Human       NLQVLNLSYNLLGELYSSNFYGLP      360
Bovine      NLQVLNLSYNLLGELYSSNFYGLP      360
Mouse       SLQVLNLSYNLLGELYNSNFYGLP      361
Chicken     NLEILNLSSNLLGELYDYTFEGLH      362
Zebrafish   HLLKLNLSQNFLGSIDSRMFENLD      364

LRR13       xLxxLxLxxNxϕxxϕxxxxFxxLx
Human       KVAYIDLQKNHIAIIQDQTFKFLE      384
Bovine      KVAYIDLQKNHIAIIQDQTFKFLG      384
Mouse       RVAYVDLQRNHIGIIQDQTFRLLK      385
Chicken     SIMYIDLQQNHIGMIGEKSFSNLV      386
Zebrafish   KLEVLDLSYNHIRALGDQSFLGLP      388

LRR14       xLxxLxLxxNxϕxxϕxxxxFxxLx
Human       KLQTLDLRDNALTTIH---F--IP      403
Bovine      KLNTLDLRINALKTIY---F--LP      403
Mouse       TLQTLDLRDNALKAIG---F--IP      404
Chicken     NLKIIDLRDNAIKKLPS--F---P      405
Zebrafish   NLRKLNLTGNAVESVHT--FAALP      410

LRR15       xLxxLxLxxNxϕxxϕxxxxFxxL-x
Human       SIPDIFLSGNKL--V-T--LPKINL      423
Bovine      SIPNIFLSGNKL--M-T--LPNIPL      423
Mouse       SIQMVLLGGNKL--V-H--LPHIHF      424
Chicken     HLTSAFLSDNKL--M-S--VAHTAI      425
Zebrafish   NLNKLYLGKNRISSVSS--LPNIAH      433

LRR16       xLxxLxLxxNxϕxx---ϕxxFxx-Lx
Human       TANLIHLSENRLENLDILYFLLR-VP     448
Bovine      TANFIQLSENRLENLNDLYFLLQ-VP     448
Mouse       TANFLELSENRLENLSDLYFLLR-VP     449
Chicken     VATHIELERNWLANLGDLYVLFQ-VP     450
Zebrafish   NLSTLDLEFNKLHALSDLYTILREFP     459

LRR17       xLxxLxLxxNxϕxxϕx-xxxFxxLx
Human       HLQILILNQNRFSSCSGDQTPSENP      473
Bovine      HLQILILNQNRFSFCHQNHAPSENS      473
Mouse       QLQFLILNQNRLSSCKAAHTPSENP      474
Chicken     GVQYLLLKQNRFSYCVKHVDAIENN      475
Zebrafish   QIENIFLQGNTFSSCYNQKQIVLSD      484

LRR18       xLxxLxLxxNxϕxxϕ-----xxxxFxxLx
Human       SLEQLFLGENMLQLAWETELCWDVFEGLS    502
Bovine      SLEKLFLGENMLQLAWETGSCQDIFKGLS    502
Mouse       SLEQLFLTENMLQLAWETGLCWDVFQGLS    503
Chicken     QLIYMDLGENMLQLVWERGLCLDVFRTLS    504
Zebrafish   KLQLLHLGLSSMQLIWSEGKCLNVFADLH    513

LRR19       xLxxLxLxxNxϕxxϕxxxxFxxLx
Human       HLQVLYLNHNYLNSLPPGVFSHLT      526
Bovine      HLQLLYLNPIYLNFLPPGVFHHLT      526
Mouse       RLQILYLSNNYLNFLPPGIFNDLV      527
Chicken     KLQVLHLNNNYLSALPQEIFNGLT      528
Zebrafish   QLQQLSLTANGLQSLPKDIFKDLT      537

LRR20       xLxxLxLxxNxϕxxϕxxxxFxxLx
Human       ALRGLSLNSNRLTVLSHNDLPA        548
Bovine      ALRGLSLKDNRLTVLFPGDLPA        548
Mouse       ALRMLSLSANKLTVLSPGSLPA        549
Chicken     SLKRLNLASNLLSHLSLRVFPQ        550
Zebrafish   SLFFLDLSFNSLKYLPTDVFPK        559

LRR21       xLxxLxLxxNxϕxxϕxxxxFx
Human       NLEILDISRNQLLAPNPDVFV         569
Bovine      NLEILDISGNQLLSPDPDLFA         569
Mouse       NLEILDISRNQLFSPDPALFS         570
Chicken     SLTNLNLSGNQLFSPKPEVFM         571
Zebrafish   SLQILNLDYNSIYSVDPNLFS         580

LRR22       xLxxLxLxxNxϕ
Human       SLSVLDITHNKF                  581
Bovine      SLSAIDITHNNF                  581
Mouse       SLRVLDITHNEF                  582
Chicken     TLSILDITHNKY                  583
Zebrafish   TLSYLSLMNNDF                  592

LRRCT
Human       ICECELSTFINWLNHTNVTIAGPPADIYCVY    612
Bovine      ICECELSAFIHWLNQTNITIAGSPADMYCMY    612
Mouse       VCNCELSTFISWLNQTNVTLFGSPADVYCMY    613
Chicken     VCDCALKSLLVWLNETNVTLAGSESDRYCVY    614
Zebrafish   RCDCDLKDFQTWLNQTNVTFVHPIEDVTCAS    623

LRRCT
Human       PDSFSGVSLFSLSTEGCDEEEVLK-S--LK     639
Bovine      PNSLAGVSIYSLSTESCEEEEVLE-S--LK     639
Mouse       PNSLLGGSLYNISTEDCDEEEAMR-S--LK     640
Chicken     PPALAGVPVSFLTYDDCDEDELQQ-T--LR     641
Zebrafish   PEDQYMVPVVKSSIQ-CENEEEERRTEKLR     652
```

Fig. S3. Amino-acid sequence alignment of TLR5 ectodomains in different species.
Zebrafish TLR5 residues in the TLR5-N14$_{VLR}$/FliC-ΔD0 structure are in black and the remaining residues are in gray. TLR5/FliC interface residues are in bold and color-coded (primary interface-A, green; primary interface-B, blue; dimerization interface-α, red; dimerization interface-β, cyan), and their corresponding residues in orthologs are also colored accordingly if they are identical. Consensus LRR sequences are shown above the TLR5 sequences.

Fig. S4

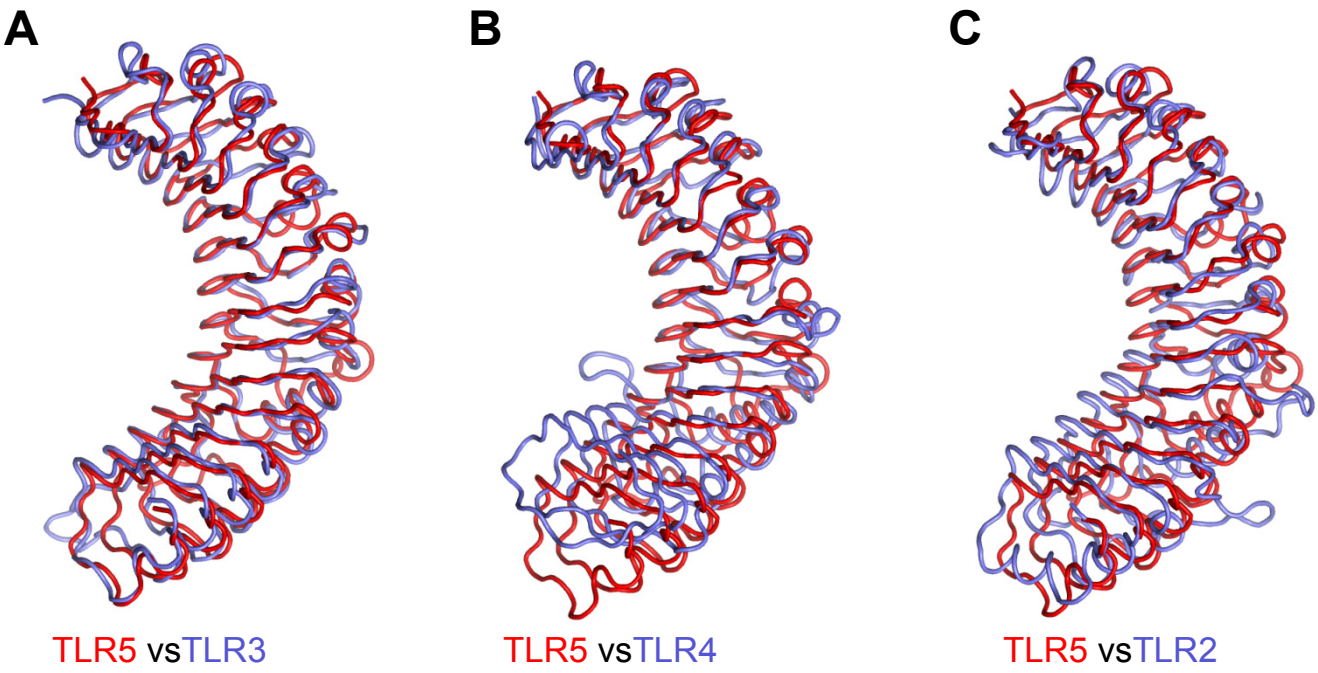

Fig. S4. TLR5-N14 folds into a single domain structure and exhibits the highest similarity with TLR3.

Among TLRs, the LRR structure of TLR5 (red) is most similar to TLR3 (RMSD, 1.7 Å for 333 Cα atoms; light blue in A) where their concave surfaces show similar radii and twists of their LRR β-strands (A). Furthermore, careful examination of LRR convex surfaces indicates that TLR5 and TLR3 display highly similar secondary and even tertiary structural folds for several of their LRR modules. In contrast, TLR5 substantially deviates from other TLRs, including TLR4 (RMSD, 2.3 Å for 263 Cα atoms; light blue in B) and TLR2 (RMSD, 2.7 Å for 300 Cα atoms; light blue in C) that contain three subdomains in their LRR folds (B and C). The TLR5-N14 structure was superimposed on structures of TLR3 (A; PDB code 2A0Z) (*56*), TLR4 (B; PDB code 2Z64) (*20*), and TLR2 (C; PDB code 2Z7X) (*4*). LRRNT-LRR14 modules of TLR structures were used in the comparison.

Fig. S5

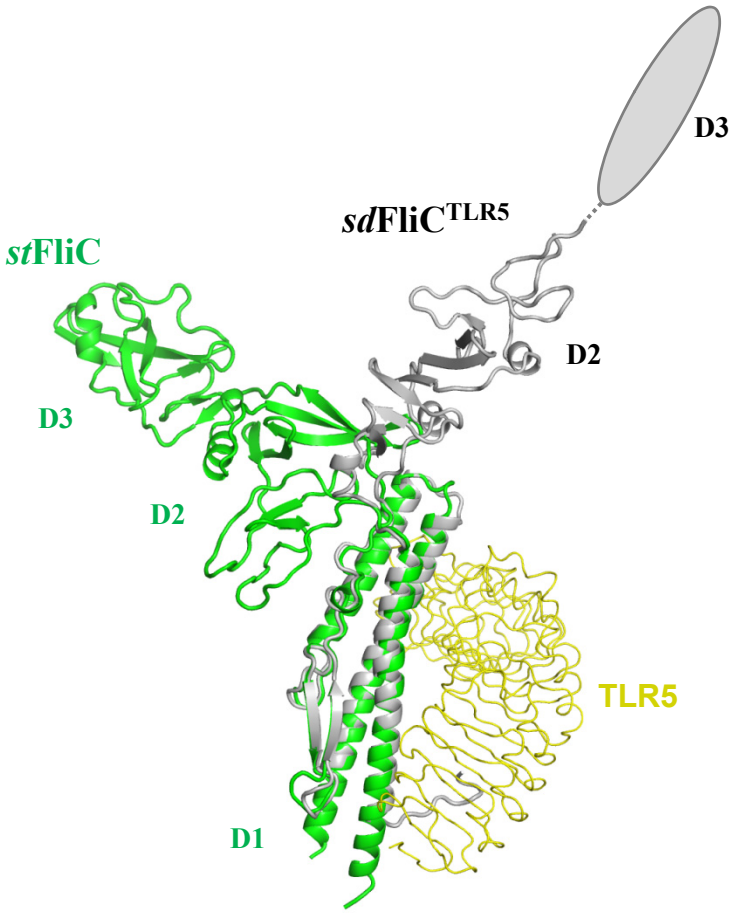

Fig. S5. FliC structure comparison between TLR5-bound *sd*FliC (*sd*FliC^{TLR5}; gray) and *Salmonella* Typhimurium FliC (*st*FliC; green; PDB code 1IO1) (*40*).
The conserved *sd*FliC D1 domain is highly similar to the corresponding domain in *st*FliC, except for the flexible C-terminal region (Cα-RMSD without C-terminal region, 1.1 Å). In the TLR5-N14$_{VLR}$/*sd*FliC-ΔD0 structure, the C-terminal region (residues 451-460) of *sd*FliC adopts an extended structure and makes contact (360 Å^2 b.s.a.) with the N-terminal LRRs of TLR5. However, the contact is not conserved in our 4.0 Å resolution structure of TLR5-N17$_{VLR}$ in complex with *st*FliC-ΔD0, suggesting that the interaction of *sd*FliC C-terminal segment with TLR5 is either *sd*FliC-specific or a result of crystal packing.
The hypervariable D2 domain of *sd*FliC exhibits a structure that differs from *st*FliC. *sd*FliC D2 domain folds into a rod shape, but that of *st*FliC D2 is a triangular shape. In *sd*FliC D2 domain, two sets of three antiparallel β-strands create a continuous β-sheet that is decorated with an α-helix at each end on the same side. The β-sheet extends to two additional antiparallel β-strands that sit on the D1 domain. Furthermore, *sd*FliC and *st*FliC are differ in D1-D2 interdomain angles. *sd*FliC D2 domain relatively straightly extends from the D1 domain, whereas *st*FliC D1 and D2 domains make a ~100˚ bend. These structure differences in the D2 domain between two phylogenetically distant groups of *Salmonella* (*57*) suggest that genes of the hypervariable domains rapidly evolved as a result of extremely low evolutionary constraints or were acquired by duplication of different genes. The D3 domain of *sd*FliC^{TLR5} could not be modeled due to its poor electron density, but a molecular envelope can be deduced from the electron density (gray ellipse).

Fig. S6

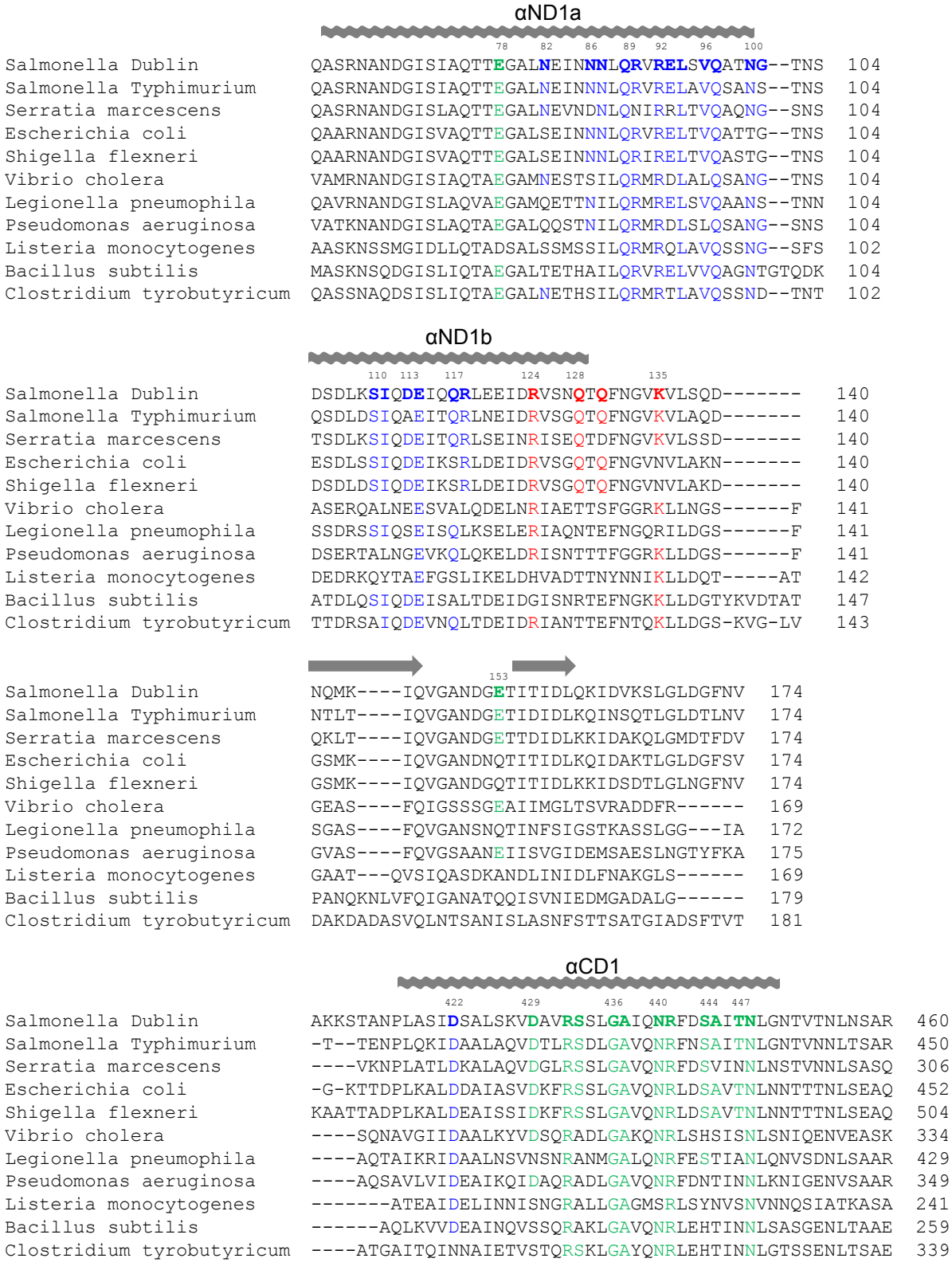

Fig. S6. Flagellin amino-acid sequence alignment.
Flagellin D1 domain sequences of β- and γ-proteobacteria were aligned by *ClustalW*. The secondary structures are shown above the sequences as waves for α-helices and arrows for β-strands. Interface residues in *sd*FliC are in bold and color-coded (primary interface-A, green; primary interface-B, blue; dimerization interface-α, red), and identical residues in other flagellin sequences are also colored accordingly.

Fig. S7

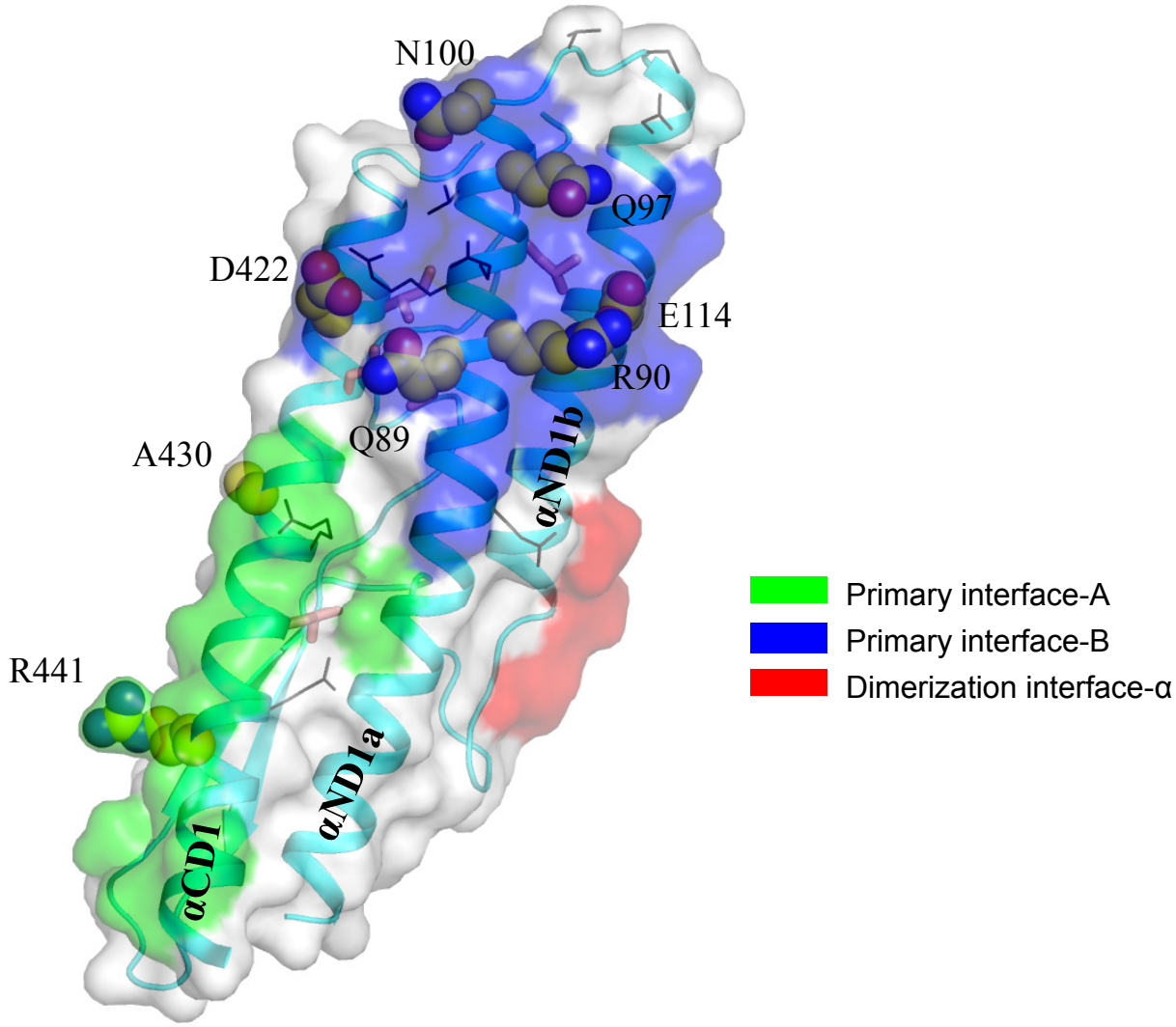

Fig. S7. TLR5/FliC interfaces (primary interface-A, green surface; primary interface-B, blue surface; dimerization interface-α, red surface) include functionally important FliC residues (exposed residues, spheres; buried hydrophobic residues, thick sticks) whose alanine mutations reduce cellular response against FliC (*11*). No effects were observed for residues shown in thin gray sticks.

Fig. S8

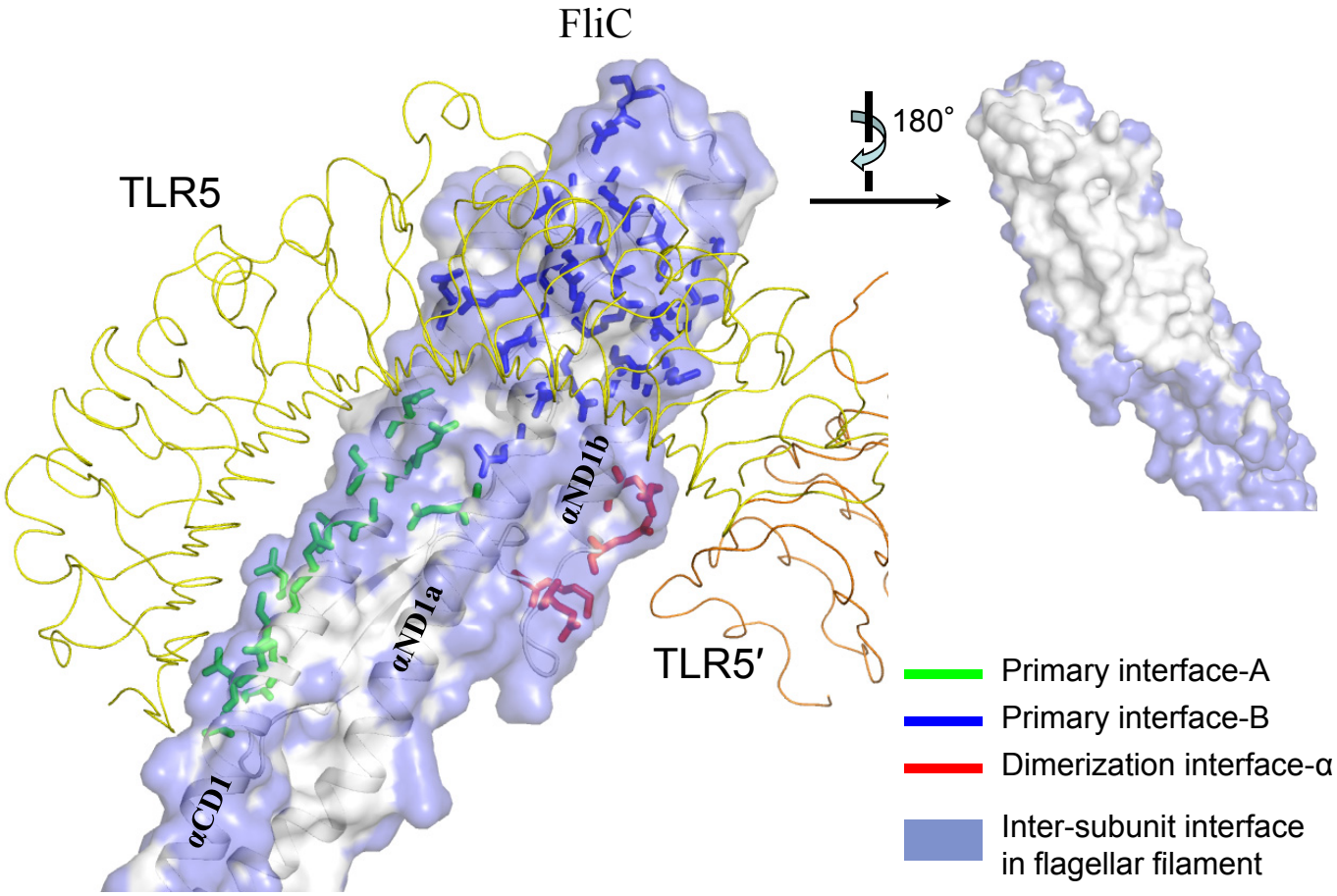

Fig. S8. TLR5 recognizes functionally important FliC residues that participate in flagellar filament formation. TLR5/FliC interface residues are shown in colored sticks (primary interface-A, green; primary interface-B, blue; dimerization interface-α, red) and FliC residues contributing to inter-subunit interaction in the flagellar filament are represented by blue surfaces (PDB code 3A5X) (*55*).

Fig. S9

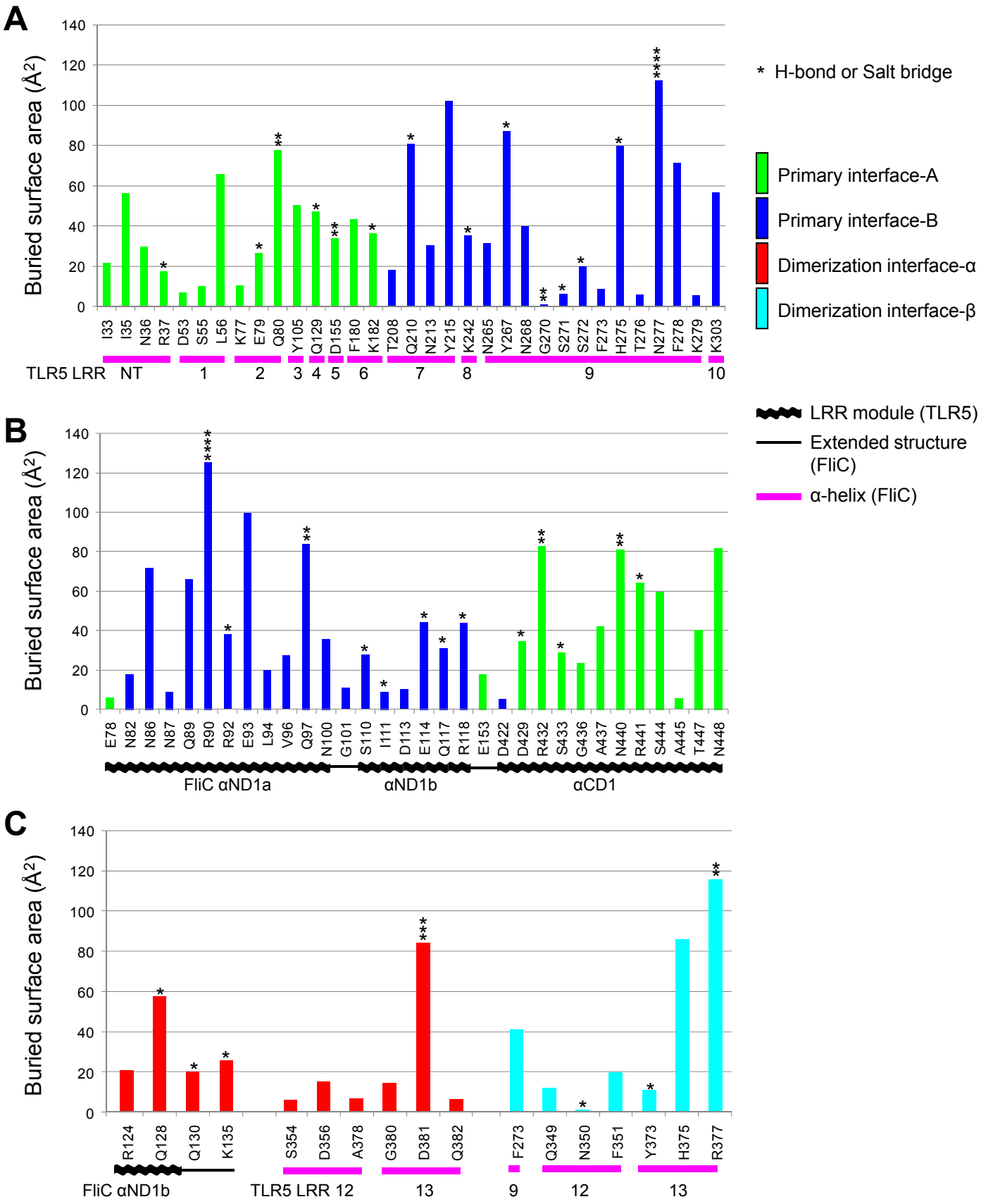

Fig. S9. Buried surface areas of the primary binding interface residues (TLR5 in A and FliC in B) and secondary dimerization interface residues (C). H-bonds or salt bridges are represented by '*' above the buried surface area bars.

Fig. S10

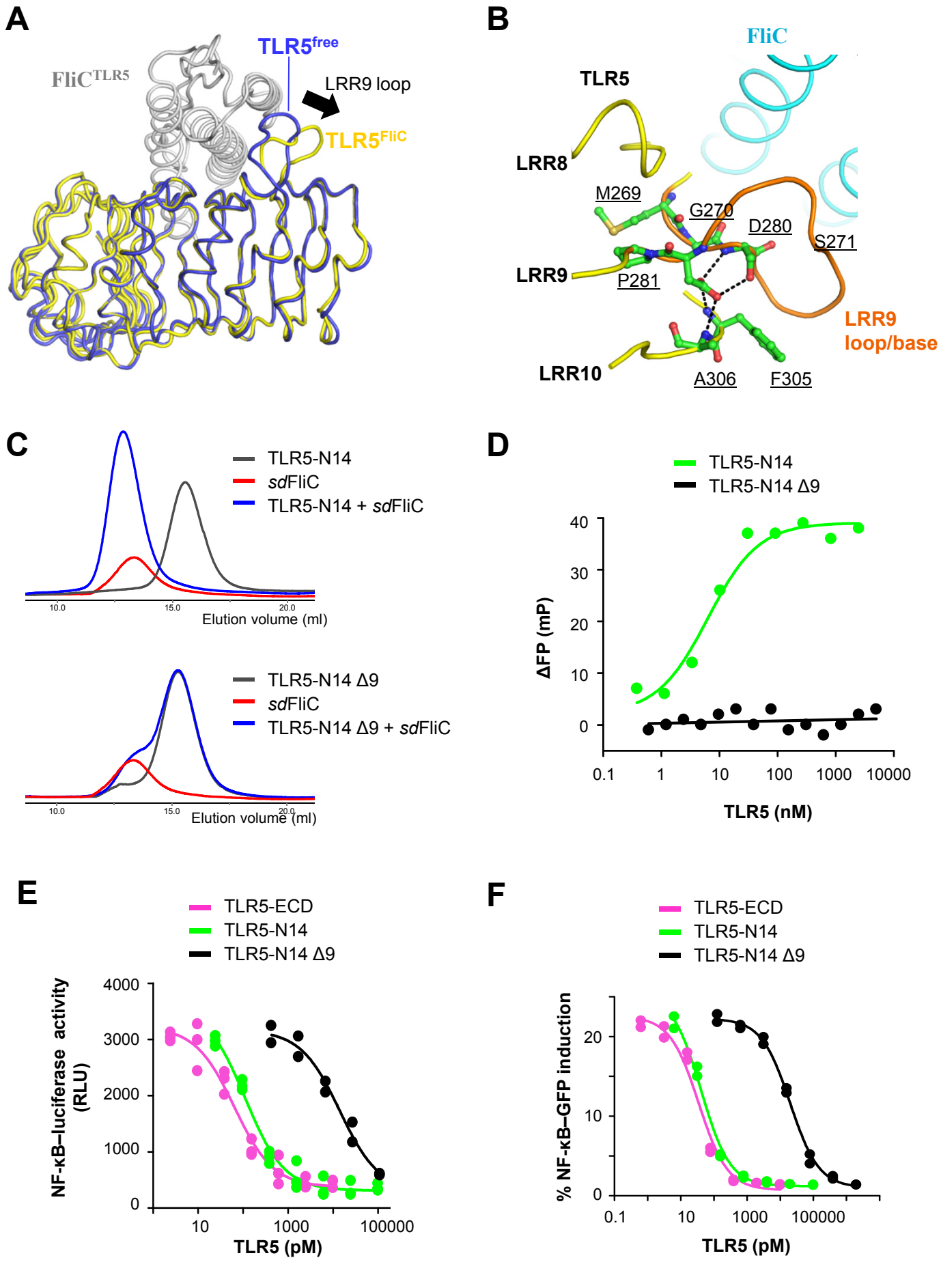
A
FliC^TLR5
TLR5^free
LRR9 loop
TLR5^FliC
B
FliC
TLR5
LRR8
M269
G270
D280
S271
LRR9
P281
LRR9 loop/base
LRR10
A306
F305
C
TLR5-N14
sdFliC
TLR5-N14 + sdFliC
10.0
15.0
20.0
Elution volume (ml)
TLR5-N14 Δ9
sdFliC
TLR5-N14 Δ9 + sdFliC
10.0
15.0
20.0
Elution volume (ml)
D
TLR5-N14
TLR5-N14 Δ9
ΔFP (mP)
40
30
20
10
0
0.1
1
10
100
1000
10000
TLR5 (nM)
E
TLR5-ECD
TLR5-N14
TLR5-N14 Δ9
NF-κB–luciferase activity (RLU)
4000
3000
2000
1000
0
10
1000
100000
TLR5 (pM)
F
TLR5-ECD
TLR5-N14
TLR5-N14 Δ9
% NF-κB–GFP induction
20
10
0
0.1
10
1000
100000
TLR5 (pM)

Fig. S10. Conformational variability of the TLR5 LRR9 loop and its critical role in FliC interaction.

(A) A protruding loop of TLR5 LRR9 undergoes conformational changes upon FliC binding. To illustrate the structural changes, the unliganded TLR5-N12$_{VLR}$ structure (TLR5^{free}; light blue) was superimposed on the TLR5-N14$_{VLR}$ structure (TLR5^{FliC}; yellow) that is bound to FliC (FliC^{TLR5}; gray).

(B) The base of the protruding loop of TLR5 LRR9 forms a rigid structure that acts as a pivot for the LRR9 loop to undergo structural rearrangement upon FliC binding. The LRR9 loop is flanked with and secured by highly conserved proximal residues, Met269, Gly270, Asp280, and Pro281, which constitute the rigid base of the loop. At the N-terminal base, Met269 is buried inside the LRR core and Gly270 seems to be selectively chosen to provide main-chain flexibility and to drive loop protrusion. Pro281 at the C-terminal base is also buried in the core and its main-chain rigidity would facilitate transition from loop structure to a regular LRR pattern. Next to Pro281, Asp280 plays a key role in stabilizing the base through a series of H-bonds with Phe305 and Ala306 at LRR10, as well as with Ser271 at the N-terminal part of the LRR9 loop. The protruding loop of LRR9 and its base are highlighted by orange color, and H-bonds that stabilize the LRR9 loop base are represented by dashed lines between TLR5 LRR9/10 residues (green ball-and-stick models).

(C) A deletion mutant that lacks the LRR9 loop demonstrates a critical role of the LRR9 loop in the TLR5/FliC interaction. To ascertain the significance of LRR9 loop in FliC binding, a LRR9 loop deletion mutant (TLR5-N14$_{VLR}$ Δ9) was generated. TLR5 LRR9 and its nearby LRR modules, LRR8 and LRR10, adopt remarkably similar conformations to those of TLR3 with an exception of the irregularly long, protruding LRR9 loop in TLR5. Thus, based on comparative structure and sequence analyses between TLR5 and TLR3, an TLR5 LRR9 loop deletion mutant was made to mimic the TLR3 structure. Residues 271-279 at the LRR9 loop were removed and base residues were substituted through G270S, D280A, and P281V mutations to provide structure stability. The effect of LRR9 loop deletion on FliC binding was analyzed by size-exclusion chromatography. TLR5-N14$_{VLR}$ shifted to a complex peak in the presence of FliC (top), whereas TLR5-N14$_{VLR}$ Δ9 was not able to form a complex with FliC in solution (bottom).

(D) TLR5-N14$_{VLR}$ Δ9 did not show any binding to fluorescein-conjugated CBLB502 (25 nM) up to 5 μM in a fluorescence polarization assay, whereas TLR5-N14$_{VLR}$ exhibited strong binding to CBLB502 (note that K_d for the TLR5-N14$_{VLR}$/CBLB502 interaction can not be derived from this direct binding assay since substantially high concentration of fluorescein-conjugated CBLB502 was inevitably used to obtain significant signals).

(E-F) The critical role of the TLR5 LRR9 loop in FliC binding is demonstrated by competitive, NF-κB-dependent luciferase (E) and GFP (F) induction assays in stable HEK293 reporter cells expressing *hs*TLR5. Deletion of the LRR9 loop in TLR5-N14$_{VLR}$ diminished CBLB502-mediated NF-κB-luciferase and NF-κB-GFP induction by 130~490 fold. CBLB502 were present in the assays at 120 pM (E) and 60 pM (F).

Fig. S11

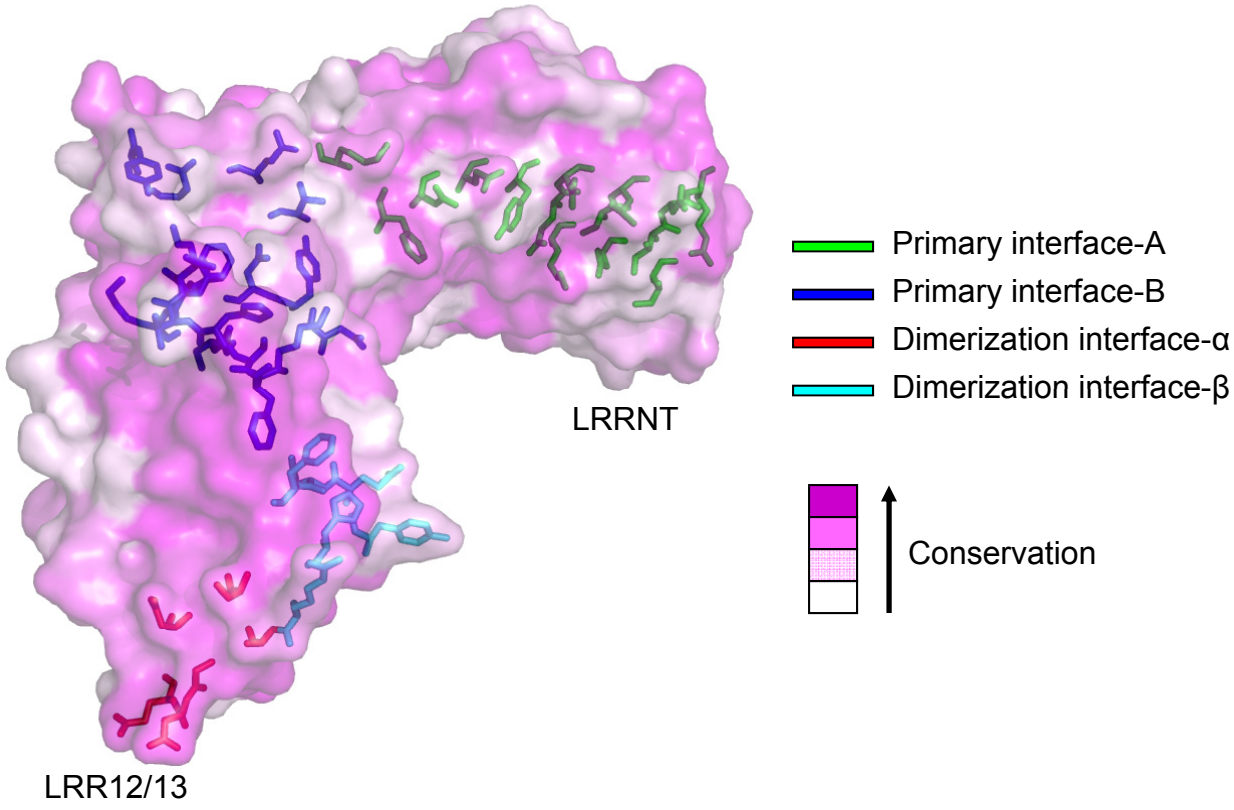

Fig. S11. Sequence conservation of TLR5 interface residues.
The sequence conservation was calculated by the ConSurf server (http://consurf.tau.ac.il/) using five TLR5 orthologs shown in fig. S3. TLR5 sequence conservation is proportional to the magenta color intensity on the TLR5 surface representation. Residues in each interface are shown by sticks in colors according to the color scheme of the figure. Interfaces-B, α, and β exhibit high sequence conservation.

Fig. S12

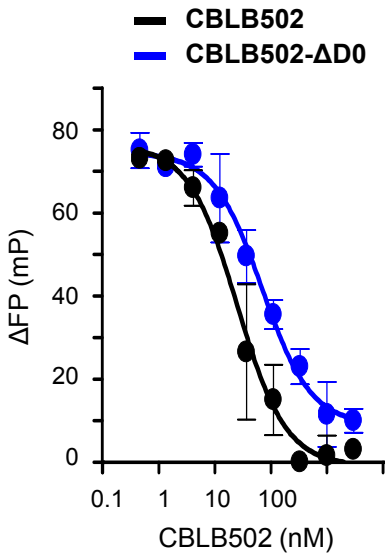

Fig. 12. A deletion of the D0 domain in CBLB502 has almost no effect on TLR5-ECD binding affinity as demonstrated by a competitive FP assay using a 1:1 mixture of 25 nM fluorescein-labeled CBLB502 and 25 nM *dr*TLR5-ECD. ΔFP signal was monitored at increasing concentrations of unlabeled CBLB502 or CBLB502-ΔD0, yielding comparable IC_{50} values (23±12 (SD) nM and 73±23 (SD) nM, respectively). Data are expressed as mean ± SD (n = 3).

Fig. S13

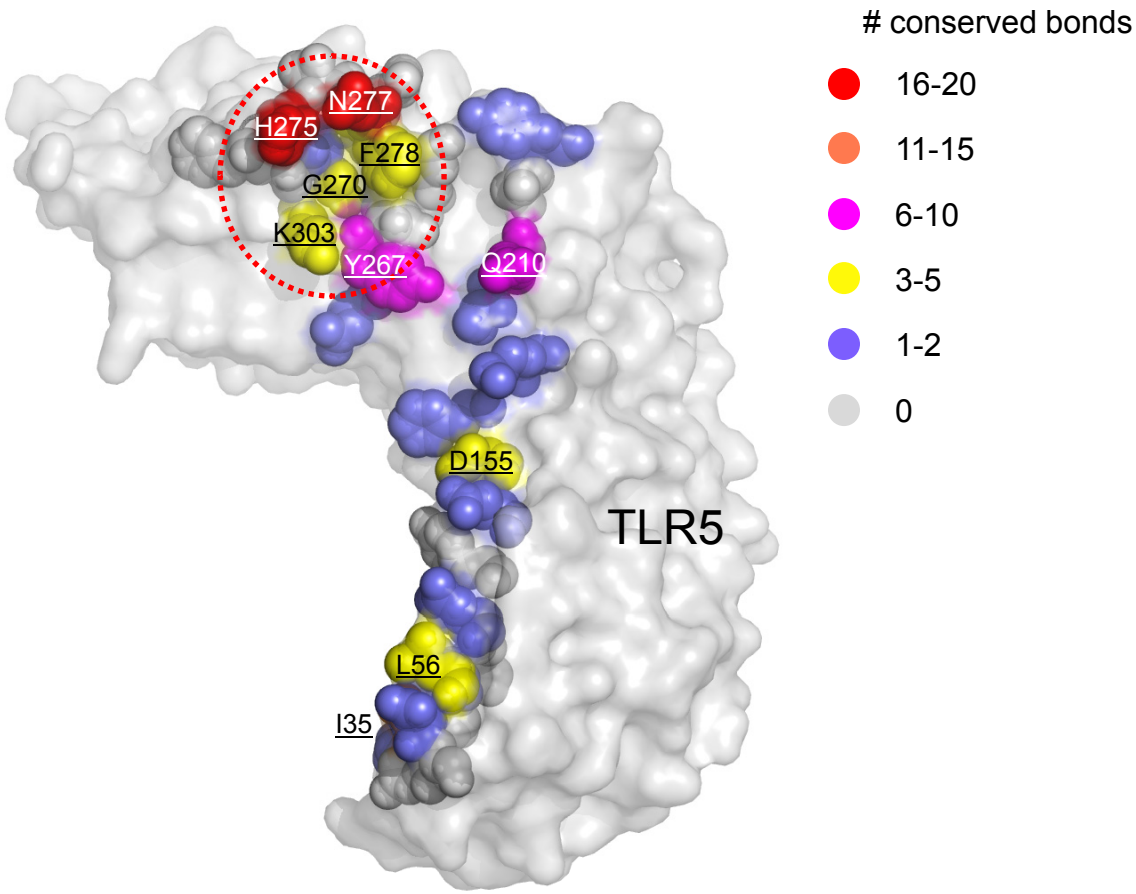

Fig. S13. Potential hot-spot for primary TLR5-FliC binding at the TLR5 LRR9 loop.
*dr*TLR5 residues involved in the primary *dr*TLR5-FliC binding are shown in spheres on the transparent surface of *dr*TLR5-N14. The number of potentially conserved interactions (H-bonds, salt bridges, and van der Waals interactions) between *dr*TLR5 and *hs*TLR5 is color-coded (16-20, red; 11-15, orange; 6-10, magenta; 3-5, yellow; 1-2, light blue; 0, gray). Interactions would be substantially more conserved in the TLR5 LRR9 loop that provides a major FliC-binding site, suggesting the potential FliC-binding hot-spot would be located at the LRR9 loop (red dotted circle).

Fig. S14

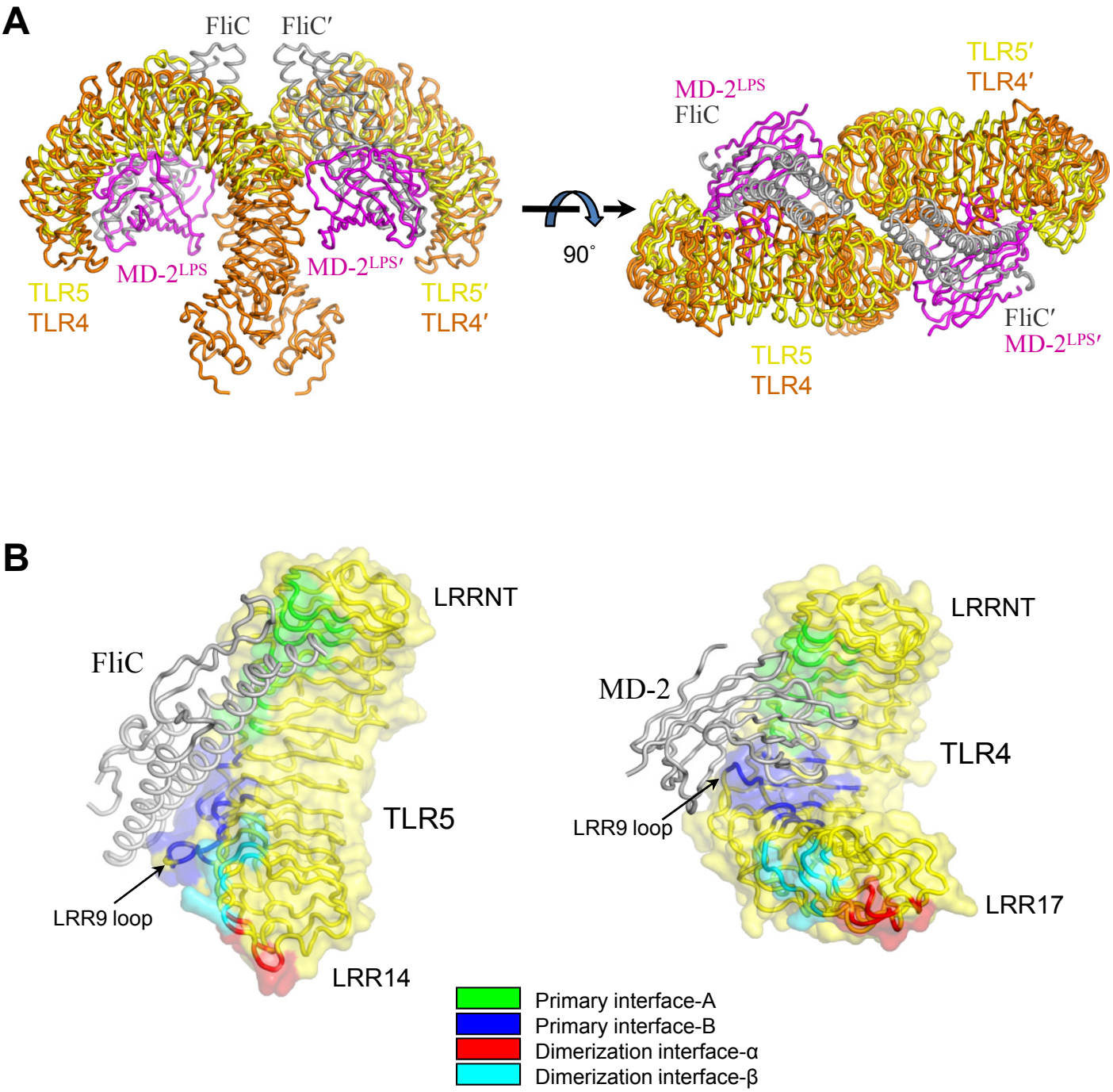

Fig. S14. Similar 2:2 quaternary assemblies for ligand-activated TLR5 and TLR4.
(A) TLR5-N14/FliC (yellow/gray) and TLR4/MD-2^{LPS} (orange/magenta; PDB code 3FXI) (*5*) exhibit similar 2:2 quaternary organization. For clarity, only FliC D1 domain is shown in the FliC structure. (B) TLR5-N14/FliC (left) and TLR4/MD-2^{LPS} (right) engages spatially similar primary and dimerization interfaces. The 1:1 complexes of TLR5/FliC (yellow/gray) and TLR4/MD-2^{LPS} (yellow/gray) are shown with each interface colored as indicated in the figure. For comparison, only LRRNT-NRR17 are illustrated for the TLR4 structure.

Table S1. Data collection and refinement statistics of TLR5 and TLR5-FliC structures.

	TLR5-N6$_{VLR}$	TLR5-N12$_{VLR}$	TLR5-N14$_{VLR}$ + *sd*FliC-ΔD0
Data Collection			
Wavelength (Å)	1.0332	0.9795	1.0332
Space group	P $6_4$22	P $4_3 2_1 2$	P $2_1 2_1 2_1$
Cell parameters			
a, *b*, *c* (Å)	86.2, 86.2, 179.4	98.3, 98.3, 195.1	58.4, 181.5, 186.4
α, β, γ (°)	90.0, 90.0, 120.0	90.0, 90.0, 90.0	90.0, 90.0, 90.0
Resolution (Å)	20.00 - 1.94 (2.01 - 1.94)[a]	20.00 - 2.83 (2.93 - 2.83)[a]	20.00 - 2.47 (2.56 - 2.47)[a]
No. observations	330,387	120,232	361,532
No. unique reflections	29,849	22,951	69,591
R_{merge} (%)[b]	5.2 (35.9)[a]	7.4 (54.4)[a]	8.6 (49.1)[a]
$I / \sigma I$	65.9 (6.8)[a]	25.9 (3.2)[a]	30.6 (4.3)[a]
Completeness (%)	99.4 (98.0)[a]	97.6 (98.9)[a]	96.8 (93.7)[a]
Redundancy	11.1 (9.3)[a]	5.3 (5.1)[a]	5.2 (4.8)[a]
Search Probes for Molecular Replacement	VLR B.61	TLR5-N6	TLR5-N12, *st*FliC-D1
Refinement			
Resolution (Å)		20.00 - 2.83	20.00 - 2.47
No. reflections (total)		21,758	66,000
No. reflections (test)		1,181	3,513
R_{cryst} (%)[c]		20.4	22.1
R_{free} (%)[d]		23.8	25.9
No. atoms			
Protein		3,146	11,017
Carbohydrate		42	154
Water		14	291
B-values (Å^2)			
TLR5$_{-VLR}$		57.3	31.0
FliC			53.8
FliC D1 domain			40.9
FliC D2 domain			73.7
Sugars		79.5	46.8
Waters		47.3	30.8
R.m.s. deviations			
Bond lengths (Å)		0.012	0.014
Bond angles (°)		1.39	1.47
Ramachandran statistics (%)[e]			
Favored		94.7	95.4
Outliers		0.0	0.0

[a]Numbers in parentheses refer to the highest resolution shell.
[b]$R_{merge} = \Sigma_{hkl}\Sigma_i | I_i(hkl) - \langle I(hkl)\rangle | / \Sigma_{hkl}\Sigma_i I_i(hkl)$
[c]$R_{cryst} = \Sigma| |F_{obs}|-|F_{calc}| | / \Sigma|F_{obs}|$ where F_{calc} and F_{obs} are the calculated and observed structure factor amplitudes, respectively
[d]R_{free} = as for R_{cryst}, but for 5% of the total reflections chosen at random and omitted from refinement
[e]Calculated using MolProbity (http://molprobity.biochem.duke.edu).

Table S2. Interface contacts observed in the TLR5-N14$_{VLR}$/FliC-ΔD0 structure.

Primary binding interface-A (b.s.a., ~530 Å^2)		**Primary binding interface-B** (b.s.a., ~790 Å^2)	
TLR5	FliC	TLR5	FliC
Ile33	Asn448	Thr208	Gln89
Ile35	Ser444, Thr447, Asn448	Gln210*	Asp422, Arg92*
Asn36	Glu153, Ala445	Asn213	Glu93
Arg37*	Asn448*	Tyr215	Val96, Gln97, Asn100, Gly101
Asp53	Thr447	Lys242*	Glu93, Gln97*
Ser55	Ser444	Asn265	Asn82, Asn86
Leu56	Arg441, Ser444	Tyr267†	Asn86, Gln89, Arg90*
Lys77	Thr447	Asn268	Arg90, Glu93
Glu79*	Asn440*	Gly270$^{\dagger\,\dagger}$	Arg90**
Gln80**	Ala437, Asn440*, Arg441*	Ser271†	Arg90*
Tyr105	Gly436, Ala437, Asn440	Ser272*	Arg118*
Gln129*	Ser433†, Ala437	Phe273	Gln117
Asp155**	Arg432**, Ser433	His275*	Asp113, Glu114, Gln117*
Phe180	Glu78, Arg432	Thr276	Ser110
Lys182*	Asp429*	Asn277†***	Leu94, Gln97*, Ser110†, Ile111†, Glu114*
		Phe278	Arg90, Glu93, Leu94, Gln97
		Lys279	Gln97
		Lys303	Asn87, Arg90, Arg118

Secondary dimerization interface-α (b.s.a., ~130 Å^2 in each of α and α′)		**Secondary dimerization interface-β** (b.s.a., ~290 Å^2)	
TLR5	FliC′	TLR5	TLR5′
Ser354	Arg124	Phe273	Phe273
Asp356	Arg124	Gln349	Arg377
Ala378	Arg124	Asn350†	Arg377*
Gly380	Gln128	Phe351	Arg377
Asp381†**	Gln128*, Gln130*, Lys135*	Tyr373†	Arg377*
Gln382	Lys135	His375	His375
		Arg377**	Gln349, Asn350†, Phe351, Tyr373†

*H-bond or salt bridge interactions that involve a side chain (n.b. multiple * or † reflect the number of H-bonds/salt bridges).

†H-bond interactions that involve a main chain.

Table S3. CBLB502 mutation analyses in TLR5 primary binding and cellular responses. To assess TLR5 primary binding, IC_{50} values were derived from a competitive fluorescence polarization assay where CBLB502 or its mutants compete with fluorescein-labeled CBLB502 for TLR5-$N14_{VLR}$ binding. To determine cellular signaling response, EC_{50} values were derived from an NF-κB-dependent luciferase reporter cell assay. The higher IC_{50} and EC_{50} values (and the lower relative IC_{50} and EC_{50} values) correspond to lower primary binding and signaling, respectively.

	IC_{50} ± SD (nM)	EC_{50} ± SD (nM)	Relative IC_{50} of mutants to CBLB502	Relative EC_{50} of mutants to CBLB502	Ratio of relative IC_{50} to relative EC_{50}
CBLB502	40 ± 7	0.077 ± 0.016	1	1	1
PIM[a]	~18000	9.5 ± 0.6	0.0022	0.0081	0.27
DIM1[b]	129 ± 25	2.4 ± 0.5	0.31	0.0323	9.6
DIM1b[c]	464 ± 41	6.8 ± 0.2	0.086	0.0011	7.6
DIM2[d]	363 ± 58	61.1 ± 9.5	0.11	0.0013	87
ΔD0	78 ± 8	82.4 ± 4.1	0.52	0.0009	550

[a]PIM: CBLB502 Q89A/R90A/Q97A
[b]DIM1: CBLB502 R124D/Q128A/Q130A/K135A
[c]DIM1b: CBLB502 R124D/Q128A/Q130E/K135E
[d]DIM2: CBLB502 Δ126-128/T129G/Q130G/K135E